The Magnetism of Monolayer FeSe in Multiple Environments

Bangjie Cao(曹邦杰)[1,2], Can Huang(黄灿)[3,4*], Lingzi Jiang(蒋灵子)[1,2], Yanfei Pan(潘燕飞)[1,2], Daning Shi(施大宁)[1,2], Jiyu Fan(樊济宇)[1,2], Chunlan Ma(马春兰)[3,4*], and Yan Zhu(朱岩)[1,2*]

[1]*College of Physics, Nanjing University of Aeronautics and Astronautics, Nanjing 211106, China*
[2]*Key Laboratory of Aerospace Information Materials and Physics, Nanjing University of Aeronautics and Astronautics, The Ministry of Industry and Information Technology, Nanjing 211106, China*
[3]*Key Laboratory of Intelligent Optoelectronic Devices and Chips of Jiangsu Higher Education Institutions, School of Physical Science and Technology, Suzhou University of Science and Technology, Suzhou 215009, China*
[4]*Advanced Technology Research Institute of Taihu Photon Center, School of Physical Science and Technology, Suzhou University of Science and Technology, Suzhou 215009, China*

(Received 25 November 2024; accepted manuscript online 9 June 2025)

FeSe is an Fe-based paramagnetic superconductor with the simplest structure. The competition between the Néel and stripe magnetic orders is believed to be one of the reasons for the absence of magnetic orders in FeSe. FeSe is recognized as a prototypical platform for competing magnetic interactions, including Néel, stripe, and staggered antiferromagnetic coupling. However, the correlations between these magnetic orders and how they change with varying environmental conditions require further study. Here, we calculated the magnetic order of monolayer FeSe in three different environments: pure one, with slight lattice distortion, and on $SrTiO_3$ substrate, by first principles calculations. We find that in the calculated dispersion relation $E(\boldsymbol{q})$ between the spin spiral energy E and spin spiral vector $\boldsymbol{q}$ of the monolayer FeSe structure, the stripe magnetic order $\boldsymbol{M}(\pi/2,\pi/2)$ has the lowest energy, and there is a flat $E(\boldsymbol{q})$ between the wave vector $\boldsymbol{X}(\pi/2,0)$ and Néel magnetic order $2\boldsymbol{X}(\pi,0)$, which are the degenerate $E(\boldsymbol{q})$ states. The ground state of $\boldsymbol{M}$ and the highest density of states around $2\boldsymbol{X}$ may be the reason for the competition of two magnetic orders. The slight lattice distortion does not alter the magnetic properties of monolayer FeSe. When monolayer FeSe is attached to the $SrTiO_3$ substrate, the degenerate $E(\boldsymbol{q})$ is still retained; meanwhile, the energy of the $2\boldsymbol{X}(\pi,0)$ state is closer to the $\boldsymbol{M}$ state, which may be one of the reasons for the increase of superconducting temperature in $FeSe/SrTiO_3$.

DOI: 10.1088/0256-307X/42/7/070714 CSTR: 32039.14.0256-307X.42.7.070714

1. Introduction. Since the discovery of Fe-based superconductors in 2008,[1,2] it has aroused the interest of countless scientists. Unlike the previously discovered high-temperature superconductors of cuprates, Fe-based superconductors overturn the widely held notion that Fe has a much more complex electronic structure and is considered to be incompatible with superconductivity.[3–14]

In these Fe-X superconductors (X = P, As, S, Se or Te),[5] FeSe is a low-toxicity model system for studying the superconducting properties of iron-based materials.[15] FeSe is composed of alternating planar layers of iron and chalcogenide, these quasi two-dimensional (2D) layers are connected by van der Waals forces.[1,12,16] The atomic and magnetic structure of FeSe is closely related to the temperature. When the temperature is down to the structural transition temperature (T_s) of 90 K, FeSe transforms from the tetragonal phase to the orthorhombic phase with a 0.3% deformation.[8,17,18] At the same time, experiments show that despite the absence of magnetic order, strong antiferromagnetic (AFM) interactions exist in FeSe and vary with temperature.[19–22] When the temperature is below the superconducting transition temperature (T_c) of 8 K, the system presents a superconducting state.[1] The relationship between structure, magnetism, and superconductivity in FeSe materials is quite unique and certainly leaves puzzles worth exploring.

One of the puzzles is the absence of magnetic order in FeSe when the temperature is below T_s, but there are still AFM spin fluctuations.[19] This paradoxical phenomenon requires a plausible explanation. The competition between the low-energy spin fluctuations associated with stripe AFM order and those associated with various types of staggered order is suggested as a possible cause for the absence of magnetic order.[21,22] Anderson pointed out that the resonating valence bond (RVB) state may provide the possibility to solve this problem.[23,24] Unfortunately, the RVB theory cannot be derived from the Hubbard-U model.[23,25] Recently, in the study of $FeCl_3$, the spiral spin liquid (SSL) state was proposed, which is a paramagnetic state associated with the degenerate propagation

*Corresponding authors. Email: canhuang@nuaa.edu.cn; wlxmcl@mail.usts.edu.cn; yzhu@nuaa.edu.cn
© 2025 Chinese Physical Society and IOP Publishing Ltd. All rights, including for text and data mining, AI training, and similar technologies, are reserved.

vector forming a continuous loop or surface in the reciprocal space.[26] SSL theory is proposed based on the J_1–J_2 Heisenberg model.[26,27] The degenerate spin spiral states could be a breakthrough point in the study of FeSe materials, where the long-range magnetic order is absent but the magnetic interaction still exists. Another interesting aspect of superconductivity is that the flat energy bands near the Fermi energy level are considered a possible explanation for high-temperature superconductivity in magic graphene.[28,29] Whether the monolayer FeSe has such a flat energy band is also a matter of concern.

FeSe has two main advantages over other Fe-based superconductors: (1) FeSe does not require doping for superconductivity.[30] Therefore, we are able to analyze the relevant properties of the system with a simple undoped structure; (2) The superconducting transition temperature of monolayer FeSe is higher than that of the bulk one.[1,15,31–36] Especially, monolayer FeSe on $SrTiO_3$ (STO) substrate achieves a T_c of 65 K.[34] This provides a good justification for studing monolayer structures in different environments. What kind of changes will appear in the magnetic properties of monolayer FeSe on STO? What kind of impact may it have on magnetic order and superconductivity? These are all issues worth exploring in depth.

Moreover, it also provides convenience for the study of magnetism and the principles behind it. At present, theoretical research on FeSe monolayer materials, especially first-principles calculations, pays more attention to the research of the ground state.[14,37,38] However, according to the SSL theory, each spin spiral state needs to be studied in depth.

The spin spiral method based on the generalized Bloch condition can explore the magnetic, atomic, and electronic structures in each spin spiral state and has been successfully applied to Rh/Gra, O/Fe(001) surface, Co/h-BN interface, Co/Pt_3 interfaces, etc.[39–43] According to this method, it is possible to study various properties of the FeSe monolayer under each spin spiral.

In this article, we use the spin-spiral method to calculate the dispersion relation $E(\boldsymbol{q})$ between the energy E and the wave vector $\boldsymbol{q}$ of the monolayer FeSe by first-principles calculation. According to the calculation results, we find that the ground state of FeSe presents a stripe AFM arrangement. The wave vector $\boldsymbol{q}$ located from $X(\pi/2, 0)$ to $2\boldsymbol{X}(\pi, 0)$ shows a length of flat $E(\boldsymbol{q})$, which has a slightly higher energy than the ground state. The $2\boldsymbol{X}(\pi, 0)$ state, shown as a Néel magnetic ordering arrangement, has a flat band in the electronic structure. In the experiment, the competition between the low-energy spin fluctuations associated with stripe AFM order and those associated with various types of staggered order is suggested as a possible cause for the absence of magnetic order.[21,22] The degenerate states between X and $2X$ provide more possibilities to explain this phenomenon. Hence, we also infer that SSL theory can be applied to FeSe materials. Moreover, the values of the $2X$ states of FeSe/STO are higher and closer to the ground M states compared to the $E(\boldsymbol{q})$ density of states in pure monolayer FeSe. FeSe/STO is more likely to exhibit a flat band $2X$ state at low temperatures, which is beneficial for improving the T_c of high-temperature superconductivity. Lattice distortion has almost no effect on the variation of magnetic exchange parameters. Although, the spin spiral energy $E(\boldsymbol{q})$ of the layered FeSe has been calculated by other studies,[44–46] our method allows us to calculate the magnetic interaction parameters of each of our nearest neighbors in detail. Moreover, we further calculate degenerate states with approximately spin spiral energy of monolayer FeSe. All these will be more helpful to the exploration of FeSe's magnetism and structure.

2. Computational Details. We adopt the first-principles calculation method under the generalized Bloch condition, which is calculated based on the Vienna *ab initio* simulation package (VASP) software of the pseudopotential plane wave method[47] of density functional theory (DFT). Besides, calculations were performed using the Perdew–Burke–Ernzerhof potential.[48] VASP can employ plane wave basis functions to solve the Kohn–Sham equation through a self-consistent iterative method and calculate the force and tensor by wave functions.[43] In order to better study the relevant properties of monolayer FeSe, we set up a vacuum layer of 20 Å to avoid structural periodicity. The convergence condition of the force was set to 5×10^{-3} eV/Å. The plane wave truncation energy is selected to be 400 eV, and the initial truncation energy is set to 300 eV to extend the plane wave function. The electron-step self-consistent calculation convergence condition is 1.0×10^{-6} eV. The GGA+U[49] method was used for calculation, and the effective onsite Coulomb interaction parameter U was set to 0.5 eV according to previous work.[50] The k-point distribution in the reciprocal lattice space is set to $12 \times 12 \times 1$. When calculating the superimposed $SrTiO_3$ substrate, van der Waals corrections were computed using the Grimme D2 method (i.e., IVDW = 1). We employed the DFT-D2 method (Grimme's van der Waals correction) as implemented in INCAR with the set IVDW = 1. Under this condition, it is ensured that the FeSe system reaches convergence.

In most past VASP calculations, the exchange interaction energy (EC) between the nearest neighbor atoms has been considered merely, and those between other farther neighbors was not obtained.[51–54] The application of the spin spiral method in VASP was by Marsman *et al.*, who calculated the spin spiral dispersion relation in γ-Fe.[55] We later utilized this method to successfully extract the RKKY interaction of Fe atoms on graphene.[56]

In order to better understand the 2D magnetic behavior observed in monolayer FeSe, Heisenberg Hamiltonian is expressed as

$$E = \sum_{0,i} \frac{1}{2} J_i (1 - \boldsymbol{s}_0 \cdot \boldsymbol{s}_i) \,, \tag{1}$$

where J_i is the nearest-neighbor exchange parameter and $\boldsymbol{s}$ is the normalized spin vector. The change of EC caused by magnetic moment rotation is the relative value compared with the ferromagnetic (FM) state, and for the convenience of discussions, the energy of the FM ground state is set as zero.[39]

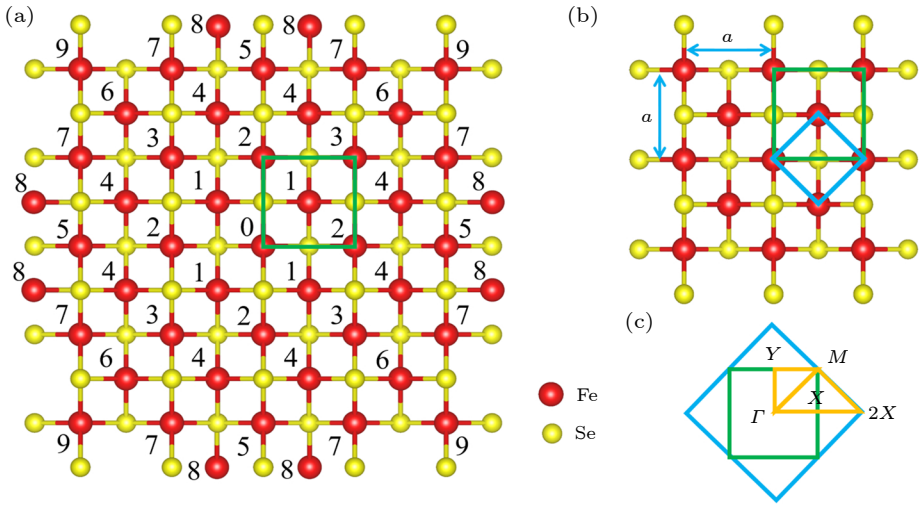

Fig. 1. (a) The arrangement diagram of the nearest neighbors of Fe atoms in monolayer FeSe. The numbers 0–9 represent the number of nearest neighbors of each Fe atom relative to the central Fe atom (labeled "0"). (b) Lattice constant, unit cell (green frame), and unit cell of the Fe atomic layer (blue frame) in monolayer FeSe. (c) The first Brillouin zone of the unit cell (green frame) and Fe atomic layer unit cell (blue frame); high-symmetric k-points in the first Brillouin zone of the Fe unit cell (M, Γ, X, Y, and $2X$) are marked relative to the FeSe unit cell.

3. Results and Discussion. As shown in Fig. 1(a), the lattice structure of FeSe is a tetragonal structure, and the Fe atom is in the center of the tetragonal Se atom. Adjacent regular tetrahedra are connected by edges; a FeSe unit cell contains two Fe atoms, and the Fe atoms interact with each other through Fe-Se bonds. After expanding the unit cell, the Fe atom labeled as "0" in Fig. 1(a) is centered, and the neighboring Fe atoms are marked with numbers. The lattice constant of a single layer of FeSe is calculated as 3.76 Å. In the Fe atom layer, the area of the unit cell formed by Fe atoms is only half that of the FeSe unit cell, as shown in Fig. 1(b). Correspondingly, the area of the first Brillouin zone of the Fe unit cell is twice that of the FeSe unit cell, as shown in Fig. 1(c).

In the tetragonal structure, the Fe atom marked "0" in Fig. 1(a) is set as the zero point, and the magnetic moment is $S(0)$. The Fe atom at the j position is denoted by $\boldsymbol{R}_j = m\boldsymbol{a}_1 + n\boldsymbol{a}_2$; among them, $\boldsymbol{a}_1$ and $\boldsymbol{a}_2$ are the base vectors. In VASP calculations, all the magnetic moments are set in the xy plane. In the generalized Bloch condition, the magnetic moment $S(\boldsymbol{R}_j)$ of the j-th adjacent Fe atom with wave vector $\boldsymbol{q}$ is

$$\begin{aligned} S(\boldsymbol{R}_j) &= S(0)\left[\sin\left(\boldsymbol{q}\cdot\boldsymbol{R}_j+\frac{\pi}{4}\right)\boldsymbol{i}+\cos\left(\boldsymbol{q}\cdot\boldsymbol{R}_j+\frac{\pi}{4}\right)\boldsymbol{j}\right] \\ &= S(0)\left\{\sin\left[2\pi(mq_1+nq_2)+\frac{\pi}{4}\right]\boldsymbol{i}\right. \\ &\quad \left.+\cos\left[2\pi(mq_1+nq_2)+\frac{\pi}{4}\right]\boldsymbol{j}\right\}. \end{aligned} \tag{2}$$

Then, according to Eq. (2), which is based on generalized Bloch conditions, considering the first to ninth nearest neighbors, the sum of EC between $S(0)$ and the magnetic moment $S(\boldsymbol{R}_j)$ of the j-th nearest neighbor is as follows:

$$\begin{aligned} E_{J_1}(\boldsymbol{q}) &= \frac{1}{2}J_1\{4-2\cos[\pi(q_1+q_2)]-2\cos[\pi(q_1-q_2)]\}, \\ E_{J_2}(\boldsymbol{q}) &= \frac{1}{2}J_2\{4-2\cos 2\pi q_1-2\cos 2\pi q_2\}, \\ E_{J_3}(\boldsymbol{q}) &= \frac{1}{2}J_3\{4-2\cos[2\pi(q_1+q_2)] \\ &\quad -2\cos[2\pi(q_1-q_2)]\}. \end{aligned} \tag{3}$$

Similar to above equations, the remaining $E_{J_4}(\boldsymbol{q})$ to $E_{J_9}(\boldsymbol{q})$ derived equations are listed in the Supplementary Materials (SM). The sum of Heisenberg interaction (HBI) energy is as follows:

$$E_{\mathrm{HBI}}(\boldsymbol{q}) = E_{J_1}(\boldsymbol{q}) + E_{J_2}(\boldsymbol{q}) + \cdots + E_{J_9}(\boldsymbol{q}). \tag{4}$$

Spin spiral dispersion relation $E(\boldsymbol{q})$ is obtained by calculations, as shown in Fig. 2(a). Figures 2(d)–2(k) show us the magnetic moment arrangements of the specially marked red points in Fig. 2(a). The highest point of energy is Γ, where the magnetic moment shows a FM arrangement. The lowest point is M, and its value relative to the FM state is −298.28 meV; the magnetic moment arrangement is shown in Fig. 1(d) as $(\pi/2, \pi/2)$ state, showing a stripe AFM arrangement.[14] Although there is controversy about the ground state of monolayer FeSe, on the premise that the lattice constant is 3.76 Å, our results show that the pair-checkerboard state is marginally higher in energy ($\Delta E = +0.0875$ meV/Fe) than the stripe AFM state. Therefore, the focus of our article remains on the stripe AFM state.[21,22] Meanwhile, it is worth noting that the energy difference between the pair-checkerboard AFM state and the stripe AFM state is closely related to the in-plane lattice constant and the on site Coulomb interaction parameter U.[37] The $(\pi, 0)$ Néel-type AFM arrangement is presented at the $2X$ point. Figure 2(a) shows that a flat $E(\boldsymbol{q})$ is generated between points X and $2X$, and the energy is close to −233.00 meV. Our calculations show that the energy of the $2X$ state is 61.19 meV higher than that of the M state. These may correspond to experimental low-energy spin fluctuations, which compete with the stripe AFM order.[21,22]

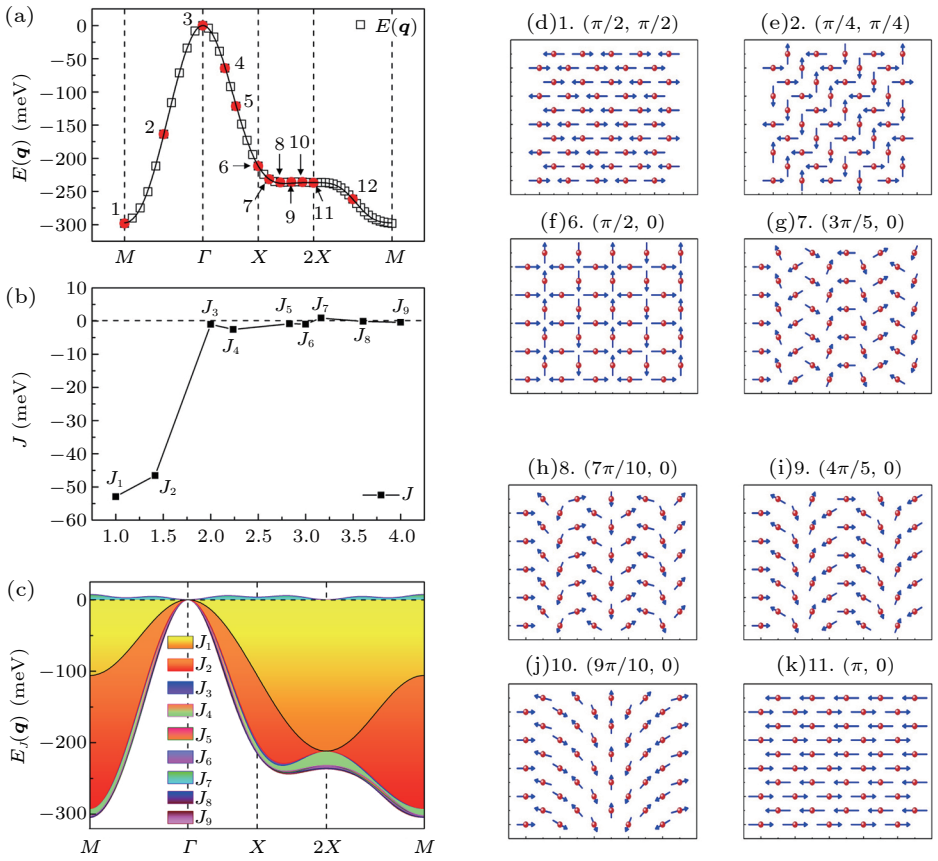

Fig. 2. (a) Spin spiral energy dispersion relation $E(\boldsymbol{q})$ of FeSe. The discrete points are calculated $E(\boldsymbol{q})$ in the FeSe system; the black solid line is the fitting curve, and the red points labeled "1–12" are the spin spiral states analyzed in detail later; M, Γ, X and $2X$ are the special k-points of the first Brillouin zone of the Fe unit cell shown in Fig. 1(c). (b) Variation trend of fitted J values of FeSe, and zero is represented by a horizontal dashed line. (c) Stacked area plot of $E_{J_i}(\boldsymbol{q})$ for EC with different J_i. (d)–(k) Magnetic moment distribution diagrams of some red points selected in (a).

The parameters J_1–J_9 of each neighborhood are obtained by least square fitting to calculated $E(\boldsymbol{q})$ with Eq. (3), as shown in Fig. 2(b). Among them, J_1 has the lowest energy of −52.90 meV, and J_2 is close to J_1, while other EC parameters are almost 0 meV. In order to reveal the contribution of each J_i $(i = 1, 2, \ldots, 9)$ to $E(\boldsymbol{q})$, we extract the relationship between each J_i and the spin spiral energy $E_J(\boldsymbol{q})$, as shown in Fig. 2(c). It can be seen that J_1 and J_2 have great contributions at X and M points respectively, while only playing an important role at the $2X$ point. In general, J_1 and J_2 play a dominant role in the monolayer FeSe structure, which satisfies the SSL theory based on J_1-J_2 model. These degenerate spin spiral states play an important role in the coexistence of Néel-type and stripe AFM states based on SSL theory.

Using these J parameters, each system can reconstruct the entire contour diagram of the spin spiral energies of the first Brillouin region, and the result is shown in Fig. 3. As can be seen from the figure, the ground state energy is concentrated at the M point, while the high energy is concentrated at the Γ point. In the four corners of the figure, that is, near the $2X$ point, unlike the other parts, no stripes are formed. The absence of fringes between X and $2X$ in Fig. 3 corresponds to the flat $E(\boldsymbol{q})$ region in Fig. 2(a).

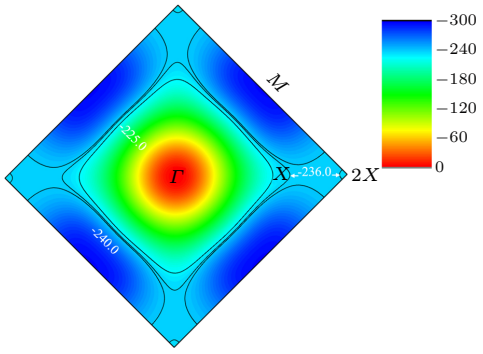

Fig. 3. Contour plot of $E(\boldsymbol{q})$ in the first Brillouin zone of Fe unit cell, the energy value corresponding to each dividing line is marked in the figure, special zone points are also marked.

The electronic state also changes with the spin spiral vector $\boldsymbol{q}$. As shown in Fig. 4(a), the d_{z^2} PDOS of Fe 3d at the Fermi level gradually converges from the extended state at the point X $(\pi/2, 0)$ to the local state at $2X$ $(\pi, 0)$ with the highest peak, and then the peak gradually becomes lower to the point of M $(\pi/2, \pi/2)$. In Figs. 4(b)–4(m), the energy band structures corresponding to these spin spiral states are plotted. The corresponding bands composed mainly of d_{z^2} are marked in red. Between the points X $(\pi/2, 0)$ and $2X$ $(\pi, 0)$, there is a nearly flat band

below the Fermi surface. The flat band may be related to the superconductivity of FeSe, which is similar to those in magic-angle graphene.[29] Meanwhile, $E(\boldsymbol{q})$ of these spin spiral structures with a flat band is roughly equal, which can be attributed to the SSL state.[26] The density of states and energy band in the ferromagnetic state also exhibit the same properties, and the results are placed in the SM.

According to previous studies, when the distortion parameter $\delta = (a-b)/(a+b)$ is about 3%, the small deformation may destroy the linear AFM state of monolayer FeSe materials. We calculate the $E(\boldsymbol{q})$ curve of monolayer FeSe under deformation and compare it with the initial structure. However, there are no significant differences in magnetism between the two structures, as shown in Fig. 5. That is to say, the possible changes in the magnetic ground state caused by deformation cannot be found from the magnetic parameters. Similar to the magnetic ground state, lattice distortion may also be a result of temperature variation, and the former should not be the reason for the latter.

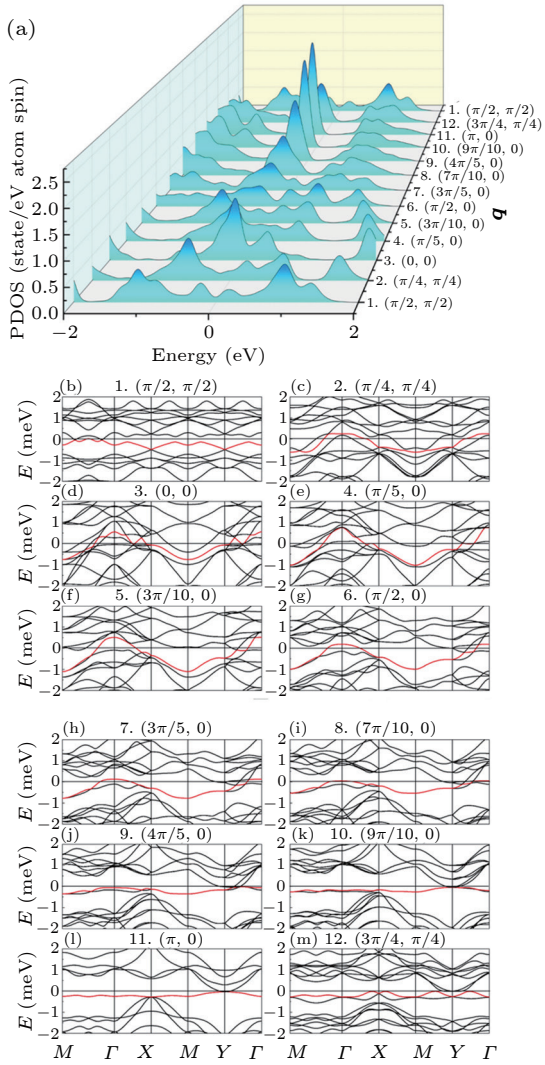

Fig. 4. (a) Calculated d_{z^2} PDOS of Fe d orbital with spin spiral states $\boldsymbol{q}$ taken from the red dots in Fig. 2(a). (b)–(m) The energy band structures of each spin spiral state in Fig. 2(a). The energy band across the Fermi surface is marked in red.

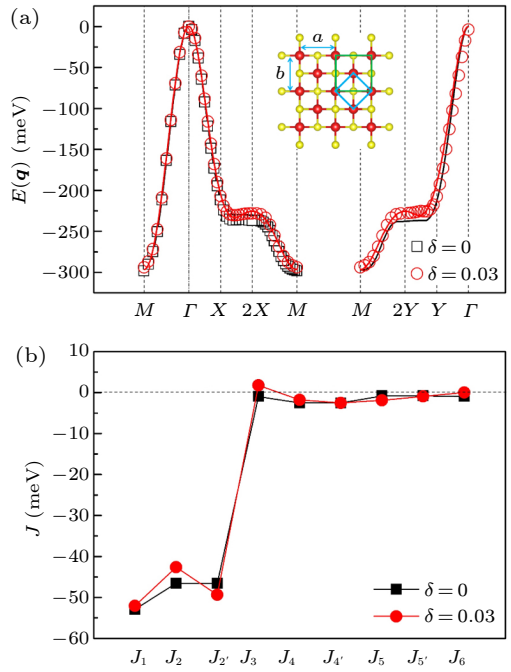

Fig. 5. (a) $E(\boldsymbol{q})$ and (b) J diagrams of deformed monolayer FeSe material; red dots represent deformed monolayer FeSe material with $\delta = 0.03$, and black boxes represent non-deformed monolayer FeSe material with $\delta = 0$ for guidance. (c) Deformed monolayer FeSe interface 2×2 top view of atomic structure; a and b represent the lattice lengths of the long and short sides of the deformation, respectively.

To investigate whether these properties of monolayer FeSe can be preserved in other environments, we designed two structures where monolayer FeSe covers the TiO layer of $SrTiO_3$, which can greatly increase the superconducting transition temperature of the monolayer FeSe.[34] There are two ways to cover FeSe on the TiO_2 layer: Se atoms near the TiO_2 layer are placed on O and Ti atoms, as shown in Figs. 6(a) and 6(b), respectively. The $E(\boldsymbol{q})$ of the two structures are named as $E(\boldsymbol{q})_{\mathrm{a}}$ and $E(\boldsymbol{q})_{\mathrm{b}}$ as shown in Fig. 6(c). Compared with the $E(\boldsymbol{q})$ without substrate in Fig. 2(a), $E(\boldsymbol{q})_{\mathrm{a}}$ and $E(\boldsymbol{q})_{\mathrm{b}}$ are basically consistent with $E(\boldsymbol{q})$. That is, the M state still has the lowest energy, and the flat $E(\boldsymbol{q})$ between X $(\pi/2, 0)$ and $2X$ $(\pi, 0)$ still exists with the substrate. Similarly, HBI parameters from the first to the ninth nearest neighbor in Fig. 6(d) are consistent in range and trend with the non-superimposed substrate structure in Fig. 2(b). Interestingly, the energy difference between $2X$ and M states is significantly reduced by the presence of the STO substrate from 61.19 to 37.70 meV in $E(\boldsymbol{q})_{\mathrm{b}}$. In addition, interfacial phonon coupling and electron doping have a crucial impact on the properties of FeSe materials,[58,59] including magnetic properties.[60] The combined effect of these two factors can easily lead to magnetic frustration between the stripe AFM state and the Néel AFM state.[61] Although we have not discussed it here, it is necessary to point it out. The $2X$ states in SSL will occupy a larger proportion with the flat bands, and this may be the reason of the higher temperature superconductivity of $FeSe/SrTiO_3$ comparing to monolayer FeSe.[34]

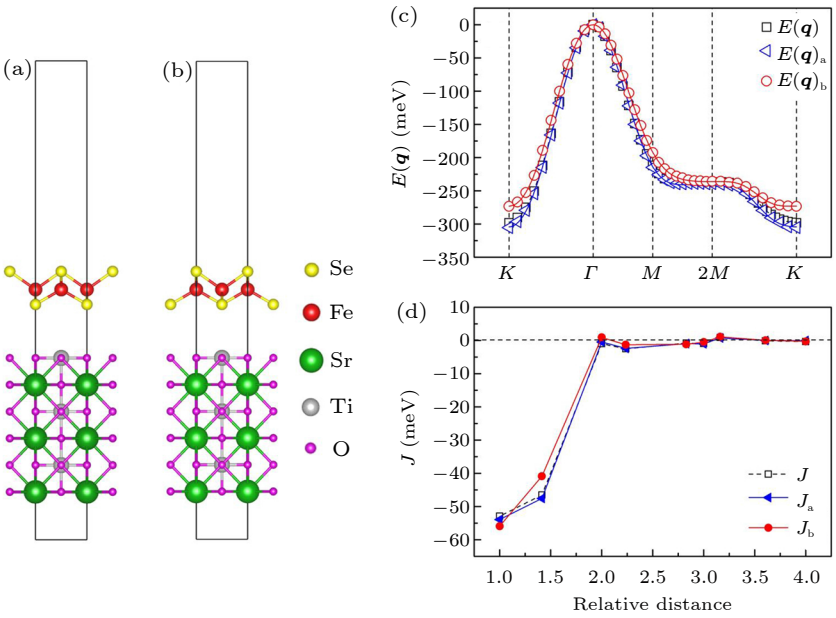

Fig. 6. (a) and (b) Two kinds of atomic structure diagrams of monolayer FeSe superimposed on the TiO_2 surface of $SrTiO_3$. (c) $E(\boldsymbol{q})$ of the two kinds of FeSe/$SrTiO_3$ structures: $E(\boldsymbol{q})_a$ and$E(\boldsymbol{q})_b$. Scatter symbols are the calculated results and lines are the fitted ones. (d) Fitted HBI parameter J values from the first to the ninth nearest neighbor of the two structures. The empty dashed line is the value of monolayer FeSe and is placed here for easy comparison.

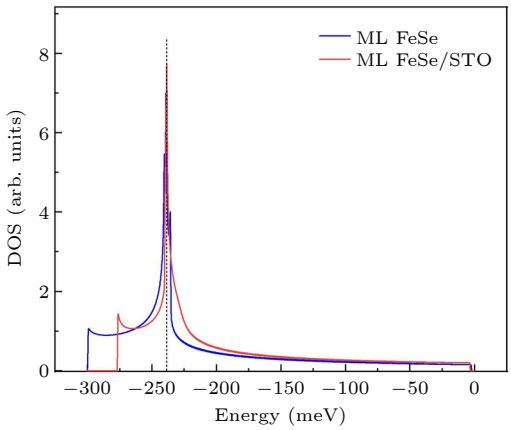

Fig. 7. DOS of different spin spiral states $E(\boldsymbol{q})$ of the monolayer FeSe structure. The blue line represents the monolayer FeSe structure, and the red line represents the structure of the monolayer FeSe superimposed on the STO substrate, as shown in Fig. 6(b).

We employ Gauss smearing methods and use the J-valued parameters in Fig. 2(b) and Fig. 6(d) to obtain the density of states (DOS) of different spin spiral states $E(\boldsymbol{q})$ in the monolayer FeSe structure. The results are shown in Fig. 7. Combined with the $E(\boldsymbol{q})$ values in Fig. 2(a) and Fig. 6(c), we can see that the two structures have the highest DOS in the vicinity of 250 meV, which is the energy level of the flat $E(\boldsymbol{q})$ state represented by the $2X$ state. Compared to pure monolayer FeSe, the energy of the $2X$ state in the FeSe/STO structure is closer to the ground state M configuration. FeSe/STO is more likely to exhibit a flat band $2X$ state at low temperatures, which is beneficial for improving the T_c of high-temperature superconductivity.[34]

4. Conclusion. Between the high symmetric $\boldsymbol{q}$-point X ($\pi/2$, 0) and $2X$ (π, 0), a flat $E(\boldsymbol{q})$ appears in FeSe. The degenerate states in the $E(\boldsymbol{q})$ flat band have slightly higher energies than the ground states with stripe AFM order, possibly corresponding to experimentally low-energy spin fluctuations that compete with the ground state. This is experimentally believed to be the cause of the absence of magnetic order in FeSe materials. Taking some spin spiral structures in this flat $E(\boldsymbol{q})$ to calculate the band structures, it is found that the band structure has a smooth band mainly composed of d_{z^2} states of the Fe atom across the Fermi energy, and this d_{z^2} band is getting flatter from point X to point $2X$. It almost becomes a straight line at the $2X$ spin spiral state. The competition of the flat band and the flat $E(\boldsymbol{q})$ between X $(\pi/2, 0)$ and $2X$ $(\pi, 0)$ may be related to the low-temperature magnetic structure and superconductivity of FeSe. Compared to pure monolayer FeSe, the energy of the $2X$ state in the FeSe/STO structure is closer to the ground state M configuration. FeSe/STO is more likely to exhibit a flat band $2X$ state at low temperatures, which is beneficial for improving the T_c of high-temperature superconductivity. Lattice distortion has almost no effect on the variation of magnetic exchange parameters.

Acknowledgements. This work was supported by the National Natural Science Foundation of China (Grant Nos. 11204131 and 11974181).

References

[1] Hsu F C, Luo J Y, Yeh K W *et al.* 2008 *Proc. Natl. Acad. Sci. USA* **105** 14262
[2] Chen W J, Tian Z J, Li P, Luo W D, and Gao C L 2017 *Phys. Rev. B* **96** 214426
[3] Sakoda M, Iida K, and Naito M 2018 *Supercond. Sci. Technol.* **31** 093001
[4] Ma F J and Lu Z Y 2008 *Phys. Rev. B* **78** 033111

[5] Liu K, Lu Z Y, and Xiang T 2012 *Phys. Rev. B* **85** 235123
[6] McQueen T M, Regulacio M, Williams A J *et al.* 2008 *Phys. Rev. B* **78** 024521
[7] Lee C H, Iyo A, Eisaki H *et al.* 2008 *Phys. Soc. Jpn.* **77** 083704
[8] Böhmer A E, Arai T, Hardy F *et al.* 2015 *Phys. Rev. Lett.* **114** 027001
[9] Paglione J and Greene R L 2010 *Nature Phys.* **6** 645
[10] Fernandes R M, VanBebber L H, Bhattacharya S *et al.* 2010 *Phys. Rev. Lett.* **105** 157003
[11] Lipscombe O J, Chen G F, Fang C *et al.* 2011 *Phys. Rev. Lett.* **106** 057004
[12] Ruiz H, Wang Y, Moritz B, Baum A, Hackl R, and Devereaux T P 2019 *Phys. Rev. B* **99** 125130
[13] Bendele M, Amato A, Conder K *et al.* 2010 *Phys. Rev. Lett.* **104** 087003
[14] Ma F J, Ji W, Hu J P, Lu Z Y, and Xiang T 2009 *Phys. Rev. Lett.* **102** 177003
[15] Wang Z Q, Liu C F, Liu Y, and Wang J 2017 *J. Phys.: Condens. Matter* **29** 153001
[16] Si Q M, Yu R, and Abrahams E 2016 *Nat. Rev. Mater.* **1** 16017
[17] Böhmer A E and Kreisel A 2017 *J. Phys.: Condens. Matter* **30** 023001
[18] Kothapalli K, Böhmer A E, Jayasekara W T *et al.* 2016 *Nat. Commun.* **7** 12728
[19] Liu K, Lu Z Y, and Xiang T 2016 *Phys. Rev. B* **93** 205154
[20] McQueen T M, Williams A J, Stephens P W *et al.* 2009 *Phys. Rev. Lett.* **103** 057002
[21] Wang Q S, Shen Y, Pan B Y *et al.* 2016 *Nat. Commun.* **7** 12182
[22] Chen T, Chen Y, Kreisel A *et al.* 2019 *Nat. Mater.* **18** 709
[23] Anderson P W 1973 *Mater. Res. Bull.* **8** 153
[24] Anderson P W 1987 *Science* **235** 1196
[25] Powell b J and McKenzie R H 2005 *Phys. Rev. Lett.* **94** 047004
[26] Gao S, McGuire M A, Liu Y H *et al.* 2022 *Phys. Rev. Lett.* **128** 227201
[27] Cao H Y, Chen S Y, Xiang H J, and Gong X G 2015 *Phys. Rev. B* **91** 020504
[28] Suárez Morell E, Correa J D, Vargas P, Pacheco M, and Barticevic Z 2010 *Phys. Rev. B* **82** 121407
[29] Y. Cao Y, V. Fatemi V, S. A. Fang S A *et al.* 2018 *Nature* **556** 80
[30] Imai T, Ahilan K, Ning F L, McQueen T M, and Cava R J 2009 *Phys. Rev. Lett.* **102** 177005
[31] Margadonna S, Takabayashi Y, Ohishi Y *et al.* 2009 *Phys. Rev. B* **80** 064506
[32] Medvedev S, McQueen T M, Troyan I A *et al.* 2009 *Nat. Mater.* **8** 630
[33] Kang B L, Shi M Z, Li S J *et al.* 2020 *Phys. Rev. Lett.* **125** 097003
[34] He S L, He J F, Zhang W H *et al.* 2013 *Nat. Mater.* **12** 605
[35] Tan S Y, Zhang Y, Xia M *et al.* 2013 *Nat. Mater.* **12** 634
[36] Zhang Y, Lee J J, Moore R G *et al.* 2016 *Phys. Rev. Lett.* **117** 117001
[37] Long X Y, Zhang S H, Wang F, and Liu Z 2020 *Npj Quantum Mater.* **5** 50
[38] Carva K, Vlaic P, and Honolka J 2022 *Nanomaterials* **12** 270
[39] Zhu Y, Fan J, and Wu R 2020 *J. Magn. Magn. Mater.* **507** 166805
[40] Zhu Y, Pan Y F, Fan J Y *et al.* 2020 *Sci. China Phys. Mech. Astron.* **63** 117511
[41] Huang C, Li X Y, Zhu Y *et al.* 2018 *Acta Phys. Sin.* **67** 117102 (in Chinese)
[42] Huang C, Jiang L Z, Zhu Y *et al.* 2021 *Phys. Chem. Chem. Phys.* **23** 22246
[43] Jiang L Z, Huang C, Zhu Y *et al.* 2022 *iScience* **25** 104039
[44] Shishidou T, Agterberg D F, and Weinert M 2018 *Commun. Phys.* **1** 8
[45] T. Olsen T 2024 *2D Mater.* **11** 033005
[46] Glasbrenner K K, Mazin I I, Harald O. Jeschke, Hirschfeld P J, Fernandes R M, and Roser Valentí 2015 *Nat. Phys.* **11** 953
[47] Kresse G and Joubert D 1999 *Phys. Rev. B* **59** 1758
[48] Perdew J P, Burke K, and Ernzerhof M 1996 *Phys. Rev. Lett.* **77** 3865
[49] Liechtenstein A I, Anisimov V I, and Zaanen J 1995 *Phys. Rev. B* **52** R5467(R)
[50] Zheng F W, Wang Z G, Kang W, and Zhang P 2013 *Sci. Rep.* **3** 2213
[51] Yang H X, Thiaville A, Rohart S, Fert A, and Chshiev M 2015 *Phys. Rev. Lett.* **115** 267210
[52] Yang H X, Boulle O, Cros V, Fert A, and Chshiev M 2018 *Sci. Rep.* **8** 12356
[53] Zhu Y, Ma C L, Shi D N, and Zhang K C 2014 *Phys. Lett. A.* **378** 2234
[54] Pan Y F, Zhu Y, Shi D N *et al.* 2015 *J. Alloys Compd.* **644** 341
[55] Marsman M and Hafner J 2002 *Phys. Rev. B* **66** 224409
[56] Zhu T, Pan Y F, Yang Z Q *et al.* 2019 *J. Phys. Chem. C* **123** 4441
[57] Liu K, Gao M, Lu Z Y, and Xiang T 2015 *Chin. Phys. B* **24** 117402
[58] Xie Y, Feng J S, Xiang H J, and Gong X G 2019 *Chin. Phys. Lett.* **36** 056801
[59] Cheng F J, Zhang Y M, Fan J Q, Song C L, Ma X C, and Xue Q K 2023 *Chin. Phys. Lett.* **40** 086801
[60] Zhou Y, Miao L, Wang P *et al.* 2018 *Phys. Rev. Lett.* **120** 097001
[61] Liu K, Zhang B J, and Lu Z Y 2015 *Phys. Rev. B* **91** 045107